

# A Magnetically and Thermally Controlled Liquid Metal Variable Stiffness Material

Mingkui Zhang, Xuanhan Chen, Yongwei Sun, Minfeng Gan, Maze Liu, Shi-Yang Tang,\* Shiwu Zhang,\* Xiangpeng Li,\* Weihua Li, and Lining Sun

Smart materials that can actively tune their stiffness are of great interest to many fields, including the construction industry, medical devices, industrial machines, and soft robotics. However, developing a material that can offer a large range of stiffness change and rapid tuning remains a challenge. Herein, a liquid metal variable stiffness material (LMVSM) that can actively and rapidly tune its stiffness by applying an external magnetic field or by changing the temperature is developed. The LMVSM is composed of three layers: a gallium–iron magnetorheological fluid (Ga–Fe MRF) layer for providing variable stiffness, a nickel–chromium wire layer for Joule heating, and a soft heat dissipation layer for accelerating heating and rapid cooling. The stiffness can be rapidly increased by 4 times upon the application of a magnetic field or 10 times by solidifying the Ga–Fe MRF. Finally, the LMVSM is attached to a pneumatically controlled soft robotic gripper to actively tune its load capacity, demonstrating its potential to be further developed into smart components that can be widely adopted by smart devices.

surgical devices,<sup>[7,8]</sup> medical implants,<sup>[9]</sup> and biosensors.<sup>[10,11]</sup> Particularly, materials with stiffness variation capability and adjustable load capacity are essential to meet complex requirements of operation for applications such as soft robots and actuators,<sup>[12–14]</sup> aerospace engineering,<sup>[15]</sup> and wearable exoskeletons.<sup>[16]</sup> Variable stiffness materials have shown promise in overcoming the trade-off between maintaining sufficient compliance and maximizing load capacity.<sup>[17]</sup>

Currently, variable stiffness materials mainly include shape memory polymers (SMP),<sup>[18,19]</sup> elastomers filled with low-melting-point alloys (LMPA),<sup>[20,21]</sup> magnetorheological elastomers/fluids (MRE/MRF),<sup>[22,23]</sup> electrorheological fluids (ERF),<sup>[24]</sup> and granular/laminar jamming structures.<sup>[25]</sup> Among them, MRF is a


smart material whose viscosity can be controlled by an external magnetic field. Upon the application of an external magnetic field, ferromagnetic particles in MRF are magnetized and arranged in an orderly manner, forming a chain-like columnar structure in the direction of the magnetic field, resulting in an increase in shear yield strength.<sup>[26]</sup> The shear yield strength of MRF can be increased by several orders of magnitude. Alternatively, LMPA such as gallium (Ga)-based alloys and Field's metal have large initial stiffness at solid state (a few

## 1. Introduction

In recent years, soft robots and actuators made of soft and programmable materials have attracted considerable attention, from academia to industry. These robots often possess unique and desirable features, such as lightweight, low cost, easy fabrication, and high compliance,<sup>[1]</sup> allowing them to be used in a wide range of applications including wearable electronics,<sup>[2,3]</sup> crawling and swimming robots,<sup>[4,5]</sup> stretchable displays,<sup>[6]</sup> minimally invasive

M. Zhang, X. Chen, M. Liu, X. Li, L. Sun  
College of Mechanical and Electrical Engineering  
Soochow University  
Suzhou 215000, China  
E-mail: licool@suda.edu.cn

Y. Sun  
Department of Orthopedics  
Xianyang First People's Hospital  
Xianyang 712000, China

 The ORCID identification number(s) for the author(s) of this article can be found under <https://doi.org/10.1002/adem.202201296>.

© 2022 The Authors. Advanced Engineering Materials published by Wiley-VCH GmbH. This is an open access article under the terms of the Creative Commons Attribution-NonCommercial License, which permits use, distribution and reproduction in any medium, provided the original work is properly cited and is not used for commercial purposes.

DOI: 10.1002/adem.202201296

M. Gan  
Department of Orthopedic  
The First Affiliated Hospital of Soochow University  
Suzhou 215000, China

S.-Y. Tang  
Department of Electronic, Electrical and Systems Engineering  
University of Birmingham  
Edgbaston, Birmingham B15 2TT, UK  
E-mail: s.tang@bham.ac.uk

S. Zhang  
CAS Key Laboratory of Mechanical Behavior and Design of Materials  
Department of Precision Machinery and Precision Instrumentation  
University of Science and Technology of China  
Hefei 230026, China  
E-mail: swzhang@ustc.edu.cn

W. Li  
School of Mechanical, Materials, Mechatronic and Biomedical Engineering  
University of Wollongong  
Wollongong, NSW 2522, Australia

GPa), and the stiffness can be reduced by millions of times after melting induced by Joule heating.<sup>[27]</sup>

In recent years, Ga-based liquid metals have received increasing attention and interest from many researchers.<sup>[28,29]</sup> Ga with a melting point of 29.8 °C, has excellent electrical/thermal conductivity, high deformability,<sup>[30,31]</sup> and large surface tension when melted.<sup>[32]</sup> Several recent works have been devoted to the characterization and applications of Ga-based metal alloys/mixtures with variable stiffness. For example, Brown et al. reported that the addition of Fe particles to eutectic gallium indium (EGaIn) liquid metal can result in an MRF.<sup>[33]</sup>

Similarly, other variable stiffness materials have been used for developing smart components in robotics. A legged robot using fast-response MRF dampers for stiffness adjustment has been demonstrated to enable real-time control during locomotion, which can improve the performance and roll-angle stability of the robot.<sup>[34]</sup> For thermally controlled materials, artificial muscles and shape-morphing mechanical metamaterials controlled by Joule heating for inducing the phase transition have been demonstrated and applied in soft robotics.<sup>[35,36]</sup> Despite these advances, research on improving the performance of soft robots enabled by materials that can be synergistically controlled using both magnetic and thermal approaches is still significantly underexplored.

In this article, we propose the liquid metal variable stiffness material (LMVSM) based on Ga metal. The material has the properties of both LMPA and MRF, i.e., its stiffness can be controlled by both temperature and magnetic field. The LMVSM has three major layers: a Joule heating layer with nickel–chromium (Ni–Cr) alloy wires embedded, a soft heat dissipation layer made of EGaIn microdroplets embedded in elastomeric composite, and a Ga–iron (Ga–Fe) MRF layer for providing variable stiffness. We conduct a series of experiments to optimize the stiffness tunability of the LMVSM and demonstrate thermal

and magnetic control of its stiffness. In addition, we use the LMVSM to manufacture soft robotic grippers with variable load capacities, demonstrating its vast potential in advancing tunable robotic devices.

## 2. Results and Discussion

### 2.1. Manufacturing Processes of the LMVSM

The processing flow for fabricating the LMVSM is shown in **Figure 1**. We first add 0.5 mL melted Ga and 0.97 g Fe particles (diameter of 48 μm) in a clean beaker. The formation of eutectic alloys requires a considerable solubility of the metals within each other. The solubility can be estimated using the Hume–Rothery rules, and most metals have a low solubility in Ga. Particularly, Fe saturates in Ga well below 1 atom%,<sup>[37]</sup> indicating that Fe particles suspended in Ga will maintain their sizes without forming eutectic alloys. Also, the Ga oxide layer tends to wet the surface of Fe particles, which further prevents the formation of alloys.<sup>[32,33]</sup>

We then add concentrated hydrochloric acid (HCl) solution (37 wt%) to the beaker to remove the oxide layer on the surface of Ga and Fe particles. As Ga and Fe particles can form a primary cell in HCl, Fe particles cannot be dissolved.<sup>[38]</sup> The mixture is vigorously stirred for 30 min until Fe particles are fully mixed with Ga, and then excess HCl solution is removed to obtain Ga–Fe MRF (Figure 1a). Next, the Ga–Fe MRF is injected and uniformly spread in a 1 mm deep Ecoflex tank (120 × 50 × 3 mm, internal groove size is 100 × 35 × 1.5 mm). The tank is made by pouring Ecoflex into a 3D-printed mold and cured for 4 h. Finally, we pour a layer of Ecoflex on the surface of Ga–Fe MRF and place a preprepared Ecoflex cap (120 × 50 × 1 mm) on it for 4 h to complete the sealing process (Figure 1a).

The Ga–Fe MRF layer is heated using a Ni–Cr alloy resistance wire (0.08 mm diameter). To increase the heat dissipation rate

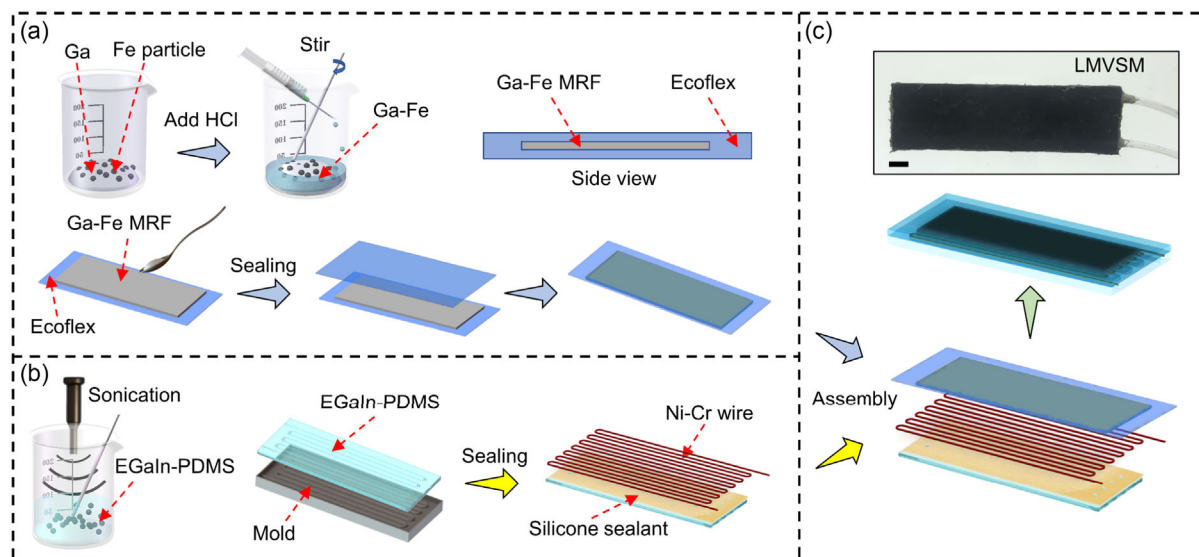


**Figure 1.** Manufacturing processes of the LMVSM. a) Flow chart and side view of the Ga–Fe MRF layer preparation. b) Flow chart of the EGaIn–PDMS heat dissipation layer preparation. c) Assembling process for making the LMVSM. The upper inset shows the actual image of the LMVSM. Scale bar is 5 mm.

during cooling, we place a channel made of EGaIn–polydimethylsiloxane (EGaIn–PDMS) composite underneath the Ni–Cr heating wire (Figure 1b). Previous works have shown that Ga and its alloys can enhance the thermal conductivity and toughness of composites.<sup>[39,40]</sup> To make the channel, EGaIn (75 wt% Ga and 25 wt% In) and PDMS (curing agent/PDMS ratio of 1:10) are placed in a plastic test tube with a weight ratio of 2:1 and stirred in a vortex mixer at a rotating speed of 2500 rpm min<sup>-1</sup> for 30 min while sonication is simultaneously performed. EGaIn can break into microdroplets during the mixing process. Next, we pour the mixture into a 3D printed serpentine-shaped channel mold (channel width of 4 mm) and vacuum it for 30 min to remove air bubbles (Figure 1b). The mold is then placed in an oven at 85 °C for 1.5 h. After demolding, the EGaIn–PDMS channel is sealed using a silicone sealant. Next, we insert 4 mm diameter tubes at each end of the channel and seal them with glue to prevent leakage. Continuous pumping of cold water in the channel can rapidly reduce the temperature of the Ga–Fe MRF layer to induce solidification. Finally, the three layers are assembled and bonded to realize the LMVSM (Figure 1c).

## 2.2. Stiffness-Tunable Behavior of the LMVSM

The LMVSM can not only adjust the stiffness by changing temperature but also has a magnetorheological effect. Figure 2a illustrates the working principle of the Ga–Fe MRF layer. Fe particles are spontaneously aligned along the magnetic flux lines to form a columnar structure, causing the material to increase its stiffness. When the magnetic field is removed, Fe particles return to a randomly distributed state, and the material reverts to a low-stiffness state.<sup>[41,42]</sup> In order to optimize the performance, we conducted a series of experiments to investigate the effects of magnetic flux density, Fe particle mass fraction, and Fe particle size on the tensile stiffness of the material. The stiffness variation test is performed by measuring the bending force under displacement, and the experiment setup is shown in Figure 2b. One end of the sample is fixed on the holder, and a connector attached to the force sensor applies a force on the other end of the sample. During the test, the connector first touches the surface of the sample and then moves downward at a speed of 0.5 mm s<sup>-1</sup>. The total bending displacement of the test is 5 mm. The force in the vertical direction is recorded by the LabVIEW program with a sampling rate of 20 Hz.

We first conduct experiments with an LMSVN sample that has the Ga–Fe MRF containing 30 wt% Fe particles (diameter of 48 μm). Figure 2c shows that the stiffness of the LMVSM reaches 1.68 N mm<sup>-1</sup> when exposed to a magnetic field with 4000 Gs magnetic flux density, which is 4 times the case when no magnetic field is applied (0.42 N mm<sup>-1</sup>). Vertical elongation of the LMVSM will cause the lateral squeeze of the Ga–Fe MRF layer (see Figure S1, Supporting Information), and the squeezing force ( $F$ ) exerted on the MRF layer can be expressed as<sup>[43]</sup>

$$F = -\frac{\pi L^4}{64} \left( \frac{6\dot{h}}{h^3} \eta(\text{Mn}) + \frac{3\rho\ddot{h}}{5h} - \frac{15\rho\dot{h}^2}{14h^2} \right) \quad (1)$$

where  $h$  and  $L$  are the thickness and the length of the Ga–Fe MRF layer, respectively (see Figure S1, Supporting Information), thus

$\dot{h}$  and  $\ddot{h}$  represent the velocity and acceleration of the Ecoflex layer that squeeze the MRF, respectively;  $\rho$  is the density of the Ga–Fe MRF; and  $\eta(\text{Mn})$  is the viscosity of the Ga–Fe MRF, which is a function of Mason number (Mn). Mn is a function of the magnetic field strength ( $H$ ), which can be expressed as<sup>[44]</sup>

$$\text{Mn}(H) = \frac{16\eta_{\text{Ga}}(\mu_{\text{Fe}} + 2\mu_{\text{Ga}})^2 \dot{\gamma}}{\mu_0 \mu_{\text{Ga}} (\mu_{\text{Fe}} - \mu_{\text{Ga}})^2 H^2} \quad (2)$$

where  $\eta_{\text{Ga}}$  is the viscosity of liquid Ga;  $\mu_0$ ,  $\mu_{\text{Ga}}$ , and  $\mu_{\text{Fe}}$  are the permeability of free space, liquid Ga, and Fe particles, respectively; and  $\dot{\gamma}$  is the fluid shear rate.  $\eta(\text{Mn})$  and Mn follow a power law relationship<sup>[44]</sup>

$$\eta(\text{Mn}) \propto \text{Mn}(H)^{-\alpha} \quad (3)$$

where  $\alpha$  is the power law exponent. When a magnetic field is applied, Fe particles align along lines of magnetic flux to form a chain structure. This reduces the Mason number, thereby increasing the viscosity of the Ga–Fe MRF to make the LMVSM stiffer.

We next measure the stiffness of the LMVSM by varying the content of Fe particles without the presence of a magnetic field, as shown in Figure 2d. The LMVSM becomes stiffer as the content of the Fe particles increases. This is because a higher content of Fe particles increases the viscosity of the Ga–Fe MRF, which leads to increased stiffness of the material.<sup>[23,24]</sup> When the Fe particle content exceeds 50%, the viscosity of the Ga–Fe MRF becomes too large to perform actual functions. As a reference, we also measured the stiffness when the Ga–Fe MRF is solidified, yielding a high stiffness of 4.03 N mm<sup>-1</sup>, which is 10 times the case when Ga–Fe MRF is liquid (Figure 2c). When exposed to a magnetic field (4000 Gs), a higher particle content leads to larger material stiffness, as shown in Figure 2e. We next test the stiffness for samples made of Fe particles (50 wt%) of different sizes (ranging from 50 nm to 74 μm) in a 4000 Gs magnetic field, as shown in Figure 2f. The result shows that there is no significant increase in stiffness when using Fe particles at the nanometer level, but the stiffness of the material increases substantially when using particles at the micrometer level.

The stiffness of the LMVSM, to a large extent, is affected more by the magnetic field and the phase of the Ga–Fe MRF, rather than the content and the size of the Fe filler particles. To better show this, we demonstrate the stiffness variation of the thermally activated LMVSM by hanging a 500 g weight on one end of the LMVSM strip. At room temperature, the Ga–Fe MRF is solid so that the LMVSM strip has sufficient stiffness to balance the 500 g weight with almost invisible deformation. When the LMVSM strip is heated to 35 °C after applying a 0.5 A current to the sandwiched Ni–Cr wire for about 60 s, the LMVSM becomes soft and can be elongated by 47%, as shown in Figure 2g. To intuitively show the effect of the magnetic field, Figure 2h shows that the LMVSM becomes softer and can be elongated by 21% upon removing the magnetic field (3000 Gs). In addition, we also test the durability of the LMVSM by repeating the elongation experiment 200 times (using a 500 g weight). We recorded the distance elongated and the position after contraction for a thermally activated sample (Figure 2i) and a magnetically activated LMVSM sample (Figure 2j). The change of length after 200 tests is

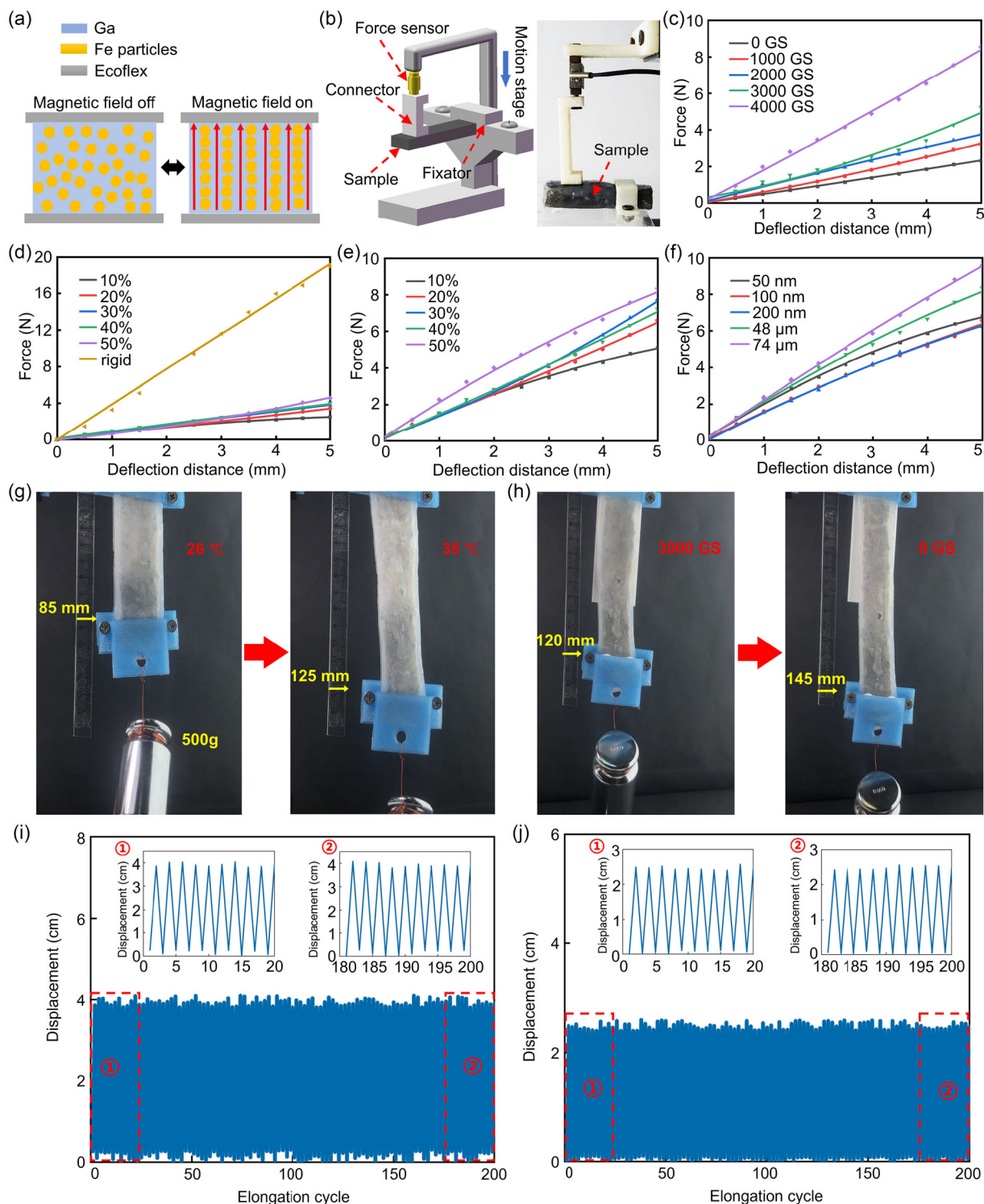


**Figure 2.** Stiffness-tunable behavior of the LMVSM. a) Working principle of the Ga–Fe MRF with variable stiffness. b) Schematic diagram and actual image of the device for stiffness testing. c) Force versus deflection plots for a LMVSM sample under magnetic fields with different magnetic flux densities (Fe particle size: 48 μm, 30 wt%). d) Force versus deflection plots for samples with different Fe particle contents (Fe particle size: 48 μm). No magnetic field is applied. The yellow line shows the plot when the Ga–Fe MRF is solidified. e) Force versus deflection plots for samples with different Fe particle contents (Fe particle size: 48 μm) when exposed to a magnetic field (4000 Gs). f) Force versus deflection plots for samples made by Fe particles (50 wt%) with different sizes. g) Demonstration of the stiffness variation of a thermally activated LMVSM sample. h) Demonstration of the stiffness variation of a magnetically activated LMVSM sample. Cyclic displacement–time curves of i) a thermally activated LMVSM sample and j) a magnetically activated LMVSM sample.

negligible, indicating that the LMVSM exhibits excellent durability (see the detailed experiment in Figure S2, Supporting Information). Ignoring the Ni–Cr wire, we can calculate the equivalent Young's modulus of the LMVSM ( $E_{LMVSM}$ ) based on the rule of mixtures, which is expressed as

$$E_{LMVSM} = E_{GaFe-Eco} \varphi_{GaFe-Eco} + E_{EGaIn-PDMS} (1 - \varphi_{GaFe-Eco}) \quad (4)$$

where  $E_{GaFe-Eco}$  and  $E_{EGaIn-PDMS}$  are the equivalent Young's moduli of the upper Ecoflex-covered Ga–Fe MRF and the lower EGaIn–PDMS composite layer, respectively; and  $\varphi_{GaFe-Eco}$  is the volume fraction of the upper Ecoflex-covered Ga–Fe MRF layer. Similarly,  $E_{GaFe-Eco}$  can be calculated as

$$E_{GaFe-Eco} = E_{GaFe} \varphi_{GaFe} + E_{Ecoflex} (1 - \varphi_{GaFe}) \quad (5)$$

where  $E_{GaFe}$  and  $E_{Ecoflex}$  are the Young's moduli of the Ga–Fe MRF and Ecoflex, respectively; and  $\varphi_{GaFe}$  is the volume fraction of the Ga–Fe MRF. When the Ga–Fe MRF is solid, for the case of spherical Fe filler particles,  $E_{GaFe}$  can be estimated as<sup>[45,46]</sup>

$$E_{GaFe} = E_{Ga} \frac{E_{Fe}(1 + \varphi_{Fe}) + E_{Ga}(1 - \varphi_{Fe})}{E_{Fe}(1 - \varphi_{Fe}) + E_{Ga}(1 + \varphi_{Fe})} \quad (6)$$

where  $E_{Ga}$  and  $E_{Fe}$  are the Young's moduli of solid Ga and Fe filler, respectively; and  $\varphi_{Fe}$  is the volume fraction of the Fe particle filler in the Ga–Fe MRF. When the Ga–Fe MRF is melted, the modulus of the layer is mainly contributed by the Ecoflex. Finally,  $E_{EGaIn-PDMS}$  can be calculated using a modified Eshelby theory that takes surface tension ( $\gamma$ ) of the EGaIn droplets into consideration<sup>[47]</sup>

$$E_{EGaIn-PDMS} = E_{PDMS} \left[ \frac{1 + \frac{5\gamma}{2E_{PDMS}R}}{(1 - \varphi_{EGaIn}) \frac{5\gamma}{2E_{PDMS}R} + (1 + \frac{5\varphi_{EGaIn}}{3})} \right] \quad (7)$$

where  $E_{PDMS}$  is the Young's modulus of PDMS,  $\varphi_{EGaIn}$  is the volume fraction of EGaIn droplets in the composite, and  $R$  is the EGaIn droplet radius.

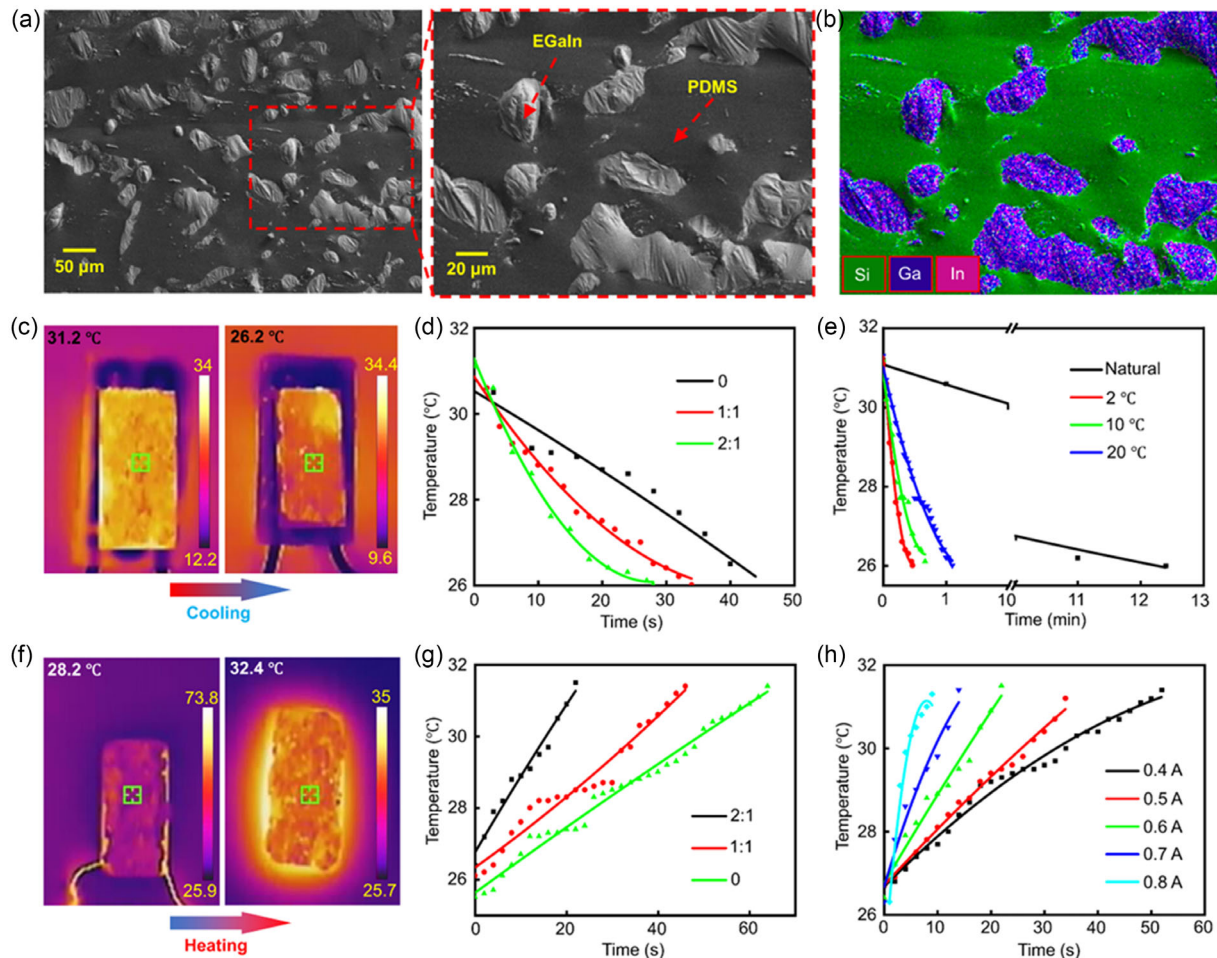


**Figure 3.** Characterization of heating and cooling efficiency. a) SEM images of the EGaIn–PDMS composite material. b) EDS element mapping of the EGaIn–PDMS composite. c) Thermal images of the LMVSM during cooling. d) Temperature versus time plots during cooling for LMVSM samples prepared by EGaIn–PDMS composites with different EGaIn:PDMS mass ratios. e) Temperature versus time plots for a LMVSM sample cooled by water coolants of different temperatures. f) Thermal images of the LMVSM during heating. g) Temperature versus time plots during heating for LMVSM samples prepared by EGaIn–PDMS composites with different EGaIn:PDMS mass ratios. h) Temperature versus time plots for a LMVSM sample heated by applying different levels of current to the Ni–Cr wire.

### 2.3. Characterization of Heating and Cooling Efficiency

An EGaIn–PDMS composite layer with a channel embedded is used to achieve fast cooling of the LMVSM to solidify Ga–Fe MRF (see Figure 1b). Figure 3a shows the scanning electron microscopy (SEM) images of the EGaIn–PDMS composite material (EGaIn:PDMS = 2:1 by weight), in which we can see that bulk EGaIn breaks into microdroplets during the mixing process, distributing uniformly within the composite. The corresponding EDS element mapping of Ga, silicon (Si), and In is given in Figure 3b. We investigate the effect of the EGaIn–PDMS ratio on the heating and cooling rate by monitoring the temperature variations of the LMVSM. Visual thermography is used to observe the temperature change at the center of the innermost surface of the LMVSM (the Ecoflex layer is peeled off from the material surface). As shown in Figure 3c, the temperature of the LMVSM can rapidly decrease by pumping cold water through the EGaIn–PDMS composite layer. Our measurements show that Ga–Fe MRF melts at  $\approx 31^\circ\text{C}$  and solidifies at  $\approx 26.5^\circ\text{C}$ . The hysteresis is probably due to uneven heating/cooling of the material and the supercooling effect of Ga metal.<sup>[48]</sup> Figure 3d shows that by pumping water ( $10^\circ\text{C}$ ) at the flow rate of  $60\text{ mL min}^{-1}$  through the EGaIn–PDMS composite layer, the time needs to cool the LMVSM from  $31$  to  $26^\circ\text{C}$  is reduced from  $44$  to  $28\text{ s}$  by increasing the EGaIn:PDMS weight ratio from  $0$  to  $2$ . The addition of EGaIn (thermal conductivity of  $26.6\text{ W m}^{-1}\text{K}^{-1}$ ) greatly improves the thermal conductivity but does not affect the flexibility of the composite.<sup>[41]</sup> To characterize the cooling rate, we conducted tests by using water with different temperatures ( $2$ ,  $10$ , and  $20^\circ\text{C}$ ) as a coolant, as shown in Figure 3e. The flow rate of water is maintained at

$60\text{ mL min}^{-1}$  using a peristaltic pump. As a reference, we also test the natural convection cooling without pumping water. Compared with natural convection cooling which requires  $\approx 12.4\text{ min}$  to cool the LMVSM from  $31$  to  $26^\circ\text{C}$ , the cooling speed is increased 25 times by using water with a temperature of  $2^\circ\text{C}$ .

Similarly, we also characterize the heating rate upon activating the Ni–Cr heater using visual thermography, as shown in Figure 3f. Upon activating the heater using a  $0.6\text{ A}$  current, the time required to heat the LMVSM from  $26$  to  $31^\circ\text{C}$  is reduced from  $64$  to  $22\text{ s}$  by increasing the EGaIn:PDMS ratio from  $0$  to  $2$ , as shown in Figure 3g. The heating rate of the LMVSM is positively correlated with the amount of EGaIn in the EGaIn–PDMS composite. Increasing the amount of EGaIn (specific heat capacity of  $\approx 468\text{ J kg}^{-1}\text{K}$ )<sup>[49]</sup> reduces the overall specific heat capacity of the composite (from  $1460\text{ J kg}^{-1}\text{K}$  for PDMS to  $\approx 727.84\text{ J kg}^{-1}\text{K}$  for the EGaIn–PDMS composite) with a mass ratio of  $2:1$  (detailed calculation and formula are given in Table S1, Supporting Information). Therefore, under the same conditions, the EGaIn–PDMS composite with a lower heat capacity can lead to a faster temperature rise to reach thermal stability. We further investigate the effect of the applied current on the heating rate. As shown in Figure 3h, the time required to heat the LMVSM from  $26$  to  $31^\circ\text{C}$  is reduced from  $52$  to  $9\text{ s}$  by increasing the current from  $0.4$  to  $0.8\text{ A}$ . In general, the current can be further increased to shorten the heating time, but a large current may cause thermal damage to the Ecoflex polymer layers.

### 2.4. Application of the LMVSM in a Pneumatic Soft Actuator

To demonstrate the application of the LMVSM in soft robotics, we attach a pair of the LMVSM to a pneumatically controlled soft

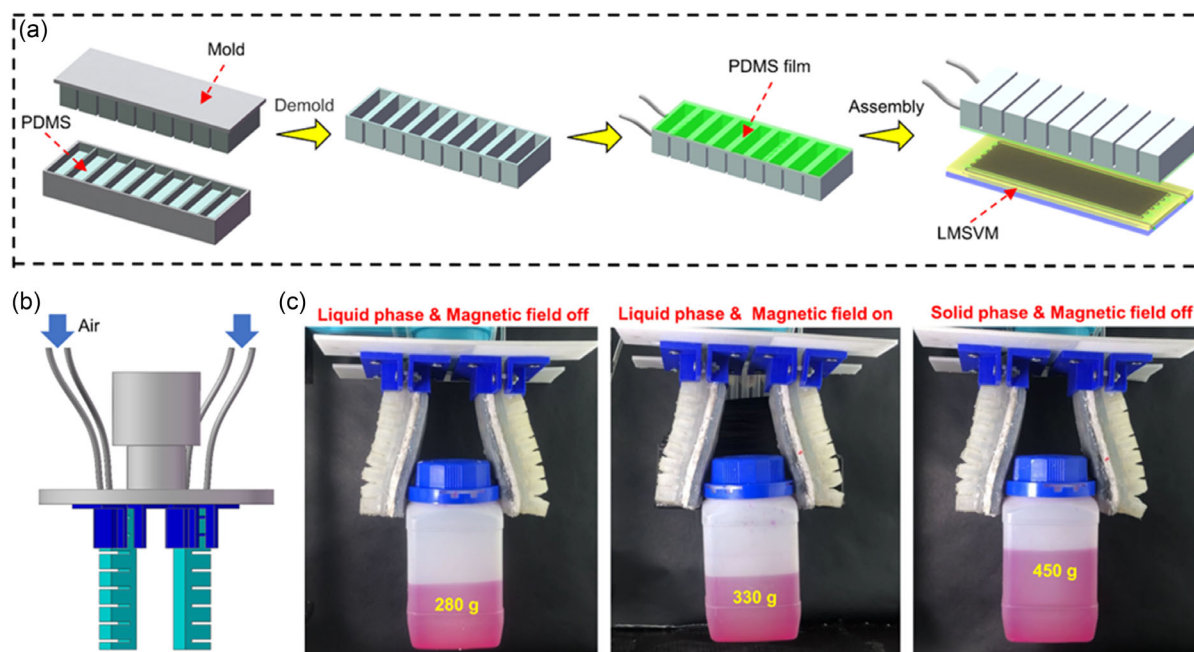


**Figure 4.** Application of the LMVSM in a pneumatically controlled soft actuator. a) Schematics showing the fabrication process of a finger of the soft gripper with variable load capacities. b) Schematic diagram of the assembled soft gripper. c) Varying the stiffness of the LMVSM allows for changing the load capacity of the soft gripper.

gripper, as shown in **Figure 4a**. The finger of the gripper is fabricated by injecting PDMS into a 3D printed mold, which is subsequently cured at 85 °C for 4 h and sealed using a PDMS film (**Figure 4a**). We insert air pipes to control the internal pressure of the chamber and realize the bending of the pneumatic actuator for grasping and releasing objects. The LMVSM is glued to the soft actuator using PDMS as the adhesive, forming a gripper with variable stiffness. Next, we assemble the gripper to a 3D-printed base, which is connected to an industrial robot arm. The schematic diagram of the device is shown in **Figure 4b**. The use of the LMVSM with variable stiffness allows us to tune the load capacity of the soft gripper without changing the pneumatic pressure. When the LMVSM is soft and no magnetic field is applied, by applying a pneumatic pressure of 5 kPa to the soft robotic gripper, the maximum grab payload is  $\approx 280$  grams (**Figure 4c**). Upon the application of a magnetic field (3000 Gs) to stiffen the LMVSM, the maximum weight that the gripper can grab increases to 330 g (**Figure 4c**). When pumping cold water to solidify the LMVSM to maximize its stiffness, the gripper is able to grab a water bottle with a weight of 450 g (**Figure 4c**). We also test the durability of the soft gripper. The gripper can complete the processes of grasping and releasing an object at least 200 times without compromising the performance (see **Figure S3**, Supporting Information, for details).

### 3. Conclusion

In summary, we develop a liquid metal variable stiffness material (LMVSM) that can adjust its stiffness by applying an external magnetic field or controlling the phase of the Ga–Fe MRF filler. The stiffness of the LMVSM can be increased by 4 times under the effect of a magnetic field and up to 10 times by reducing the temperature to solidify the Ga–Fe MRF. The Ni–Cr wire heating layer and the EGain–PDMS composite layer allow the LMVSM to possess fast heating and cooling rates, achieving stiffness change without sacrificing flexibility. The LMVSM can be attached to a pneumatically controlled soft actuator to actively adjust the load capacity, demonstrating its potential in developing smart devices with tunable properties. Moreover, the LMVSM demonstrated in this work can be further integrated into microfluidic systems to enable the development of actuators with tunable performance.<sup>[50]</sup> Such actuators could be useful for applications such as investigating mechanoresponsive properties of cells,<sup>[51]</sup> organ-on-a-chip,<sup>[52]</sup> and flow regulation.<sup>[53]</sup>

### 4. Experimental Section

**Materials and Instrument:** EGain alloy (75% Ga, 25% In) was purchased from Changsha SanTech Material Co., Ltd., all materials have a purity of 99.99%. The iron particles with a diameter from 50 nm to 80  $\mu\text{m}$  were purchased from Shanghai Yu-Sui Welding Material. SYLGARD 184 Silicone Elastomer Curing Agent and SYLGARD 184 Silicone Elastomer Base were purchased from Dow Corning, American. Ecoflex 00-30 were purchased from SMOOTH-ON, USA. The HCl solution used in this study was freshly made before all experiments. DC voltages were provided by a DC power supply (IT6432, ITECH, China). The vacuum dry oven (DZF-6050) was purchased by Shanghai Jinghong Laboratory Instrument Co., Ltd., China. The force sensor was purchased by Simbatouch Instrument Co., Ltd., China.

**Videos and Photos:** Videos were captured using an iPhone X (256GB, Apple Co., Ltd., California, USA), and the snapshots were extracted from these videos. The velocity data were obtained using a high-speed camera (HERO 5, GoPro, USA). SEM images and EDS element mappings were taken using a Merlin Compact SEM (Zeiss, Germany). The X-ray diffraction (XRD) data were obtained using an XRD system (D8 Discover Plus, Bruker, Germany) at ambient temperature.

### Supporting Information

Supporting Information is available from the Wiley Online Library or from the author.

### Acknowledgements

M.Z., X.C., and Y.S. contributed equally to this work. This work was supported in part by a grant from the NSFC under grant no. 61873339, a grant from the Natural Science Foundation of Jiangsu Province under grant no. BK20190096, a grant from the Science and Technology Projects of Suzhou under grant no. SLC201902, and supported by the State Key Laboratory of Applied Optics. S.-Y.T. is grateful for the support from the Royal Society (IEC/NSFC/201223).

### Conflict of Interest

The authors declare no conflict of interest.

### Data Availability Statement

The data that support the findings of this study are available from the corresponding author upon reasonable request.

### Keywords

liquid metals, magnetically activated, soft actuator, thermally activated, variable stiffness

Received: September 7, 2022

Revised: November 1, 2022

Published online: November 17, 2022

- [1] H. Lipson, *Soft Rob.* **2013**, *1*, 21.
- [2] T. Q. Trung, S. Ramasundaram, B.-U. Hwang, N.-E. Lee, *Adv. Mater.* **2016**, *28*, 502.
- [3] W. Zeng, L. Shu, Q. Li, S. Chen, F. Wang, X.-M. Tao, *Adv. Mater.* **2014**, *26*, 5310.
- [4] A. Villanueva, C. Smith, S. Priya, *Bioinspiration Biomimetics* **2011**, *6*, 036004.
- [5] R. F. Shepherd, F. Ilievski, W. Choi, S. A. Morin, A. A. Stokes, A. D. Mazzeo, X. Chen, M. Wang, G. M. Whitesides, *Proc. Natl. Acad. Sci. U.S.A.* **2011**, *108*, 20400.
- [6] M. S. White, M. Kaltenbrunner, E. D. Głowacki, K. Gutnichenko, G. Kettlgruber, I. Graz, S. Aazou, C. Ulbricht, D. A. M. Egbe, M. C. Miron, Z. Major, M. C. Scharber, T. Sekitani, T. Someya, S. Bauer, N. S. Sariciftci, *Nat. Photonics* **2013**, *7*, 811.
- [7] Y. J. Kim, S. Cheng, S. Kim, K. Iagnemma, *IEEE Trans. Rob.* **2013**, *29*, 1031.
- [8] M. Cianchetti, T. Ranzani, G. Gerboni, T. Nanayakkara, K. Althofer, P. Dasgupta, A. Menciassi, *Soft Rob.* **2014**, *1*, 122.

- [9] C. M. Boutry, A. Nguyen, Q. O. Lawal, A. Chortos, S. Rondeau-Gagné, Z. Bao, *Adv. Mater.* **2015**, *27*, 6954.
- [10] L. Y. Chen, B. C. K. Tee, A. L. Chortos, G. Schwartz, V. Tse, D. J. Lipomi, H. S. P. Wong, M. V. McConnell, Z. Bao, *Nat. Commun.* **2014**, *5*, 5028.
- [11] S. Lee, A. Reuveny, J. Reeder, S. Lee, H. Jin, Q. Liu, T. Yokota, T. Sekitani, T. Isoyama, Y. Abe, Z. Suo, T. Someya, *Nat. Nanotechnol.* **2016**, *11*, 472.
- [12] H. K. Yap, L. Jeong Hoon, F. Nasrallah, J. C. H. Goh, R. C. H. Yeow, presented at *2015 IEEE Int. Conf. on Robotics and Automation (ICRA)*, Seattle, WA, May **2015**.
- [13] H. K. Yap, H. Y. Ng, C.-H. Yeow, *Soft Rob.* **2016**, *3*, 144.
- [14] H. Nakai, Y. Kuniyoshi, M. Inaba, H. Inoue, in *Proc. 2002 IEEE/RSJ Int. Conf. on Intelligent Robots and Systems*, IEEE, Lausanne, Switzerland **2002**, p. 2025.
- [15] A. Y. N. Sofla, S. A. Meguid, K. T. Tan, W. K. Yeo, *Mater. Des.* **2010**, *31*, 1284.
- [16] J. H. Pikul, S. Li, H. Bai, R. T. Hanlon, I. Cohen, R. F. Shepherd, *Science* **2017**, *358*, 210.
- [17] D. J. Levine, K. T. Turner, J. H. Pikul, *Adv. Mater.* **2021**, *33*, 2007952.
- [18] K. Takashima, K. Sugitani, N. Morimoto, S. Sakaguchi, T. Noritsugu, T. Mukai, *Smart Mater. Struct.* **2014**, *23*, 125005.
- [19] Y. Yang, Y. Chen, Y. Li, M. Z. Q. Chen, Y. Wei, *Soft Rob.* **2017**, *4*, 147.
- [20] Y. Hao, T. Wang, Z. Xie, W. Sun, Z. Liu, X. Fang, M. Yang, L. Wen, *J. Micromech. Microeng.* **2018**, *28*, 024004.
- [21] I. M. Van Meerbeek, B. C. Mac Murray, J. W. Kim, S. S. Robinson, P. X. Zou, M. N. Silberstein, R. F. Shepherd, *Adv. Mater.* **2016**, *28*, 2801.
- [22] C. Majidi, R. J. Wood, *Appl. Phys. Lett.* **2010**, *97*, 164104.
- [23] M. D. Christie, S. S. Sun, D. H. Ning, H. Du, S. W. Zhang, W. H. Li, *Smart Mater. Struct.* **2016**, *26*, 015002.
- [24] A. Tonazzini, A. Sadeghi, B. Mazzolai, *Soft Rob.* **2016**, *3*, 34.
- [25] Y. S. Narang, J. J. Vlassak, R. D. Howe, *Adv. Funct. Mater.* **2018**, *28*, 1707136.
- [26] M. Lokander, B. Stenberg, *Polym. Test.* **2003**, *22*, 677.
- [27] W. Shan, T. Lu, C. Majidi, *Smart Mater. Struct.* **2013**, *22*, 085005.
- [28] J. Shu, S.-Y. Tang, Z. Feng, W. Li, X. Li, S. Zhang, *Soft Matter* **2018**, *14*, 7113.
- [29] S.-Y. Tang, V. Sivan, P. Petersen, W. Zhang, P. D. Morrison, K. Kalantar-zadeh, A. Mitchell, K. Khoshmanesh, *Adv. Funct. Mater.* **2014**, *24*, 5851.
- [30] M. D. Dickey, *Adv. Mater.* **2017**, *29*, 1606425.
- [31] S.-Y. Tang, I. D. Joshipura, Y. Lin, K. Kalantar-Zadeh, A. Mitchell, K. Khoshmanesh, M. D. Dickey, *Adv. Mater.* **2016**, *28*, 604.
- [32] T. Daeneke, K. Khoshmanesh, N. Mahmood, I. A. de Castro, D. Esrafilzadeh, S. J. Barrow, M. D. Dickey, K. Kalantar-zadeh, *Chem. Soc. Rev.* **2018**, *47*, 4073.
- [33] F. Carle, K. Bai, J. Casara, K. Vanderlick, E. Brown, *Phys. Rev. Fluids* **2017**, *2*, 013301.
- [34] M. D. Christie, S. Sun, L. Deng, H. Du, S. W. Zhang, W. H. Li, *Smart Mater. Struct.* **2022**, *31*, 045003.
- [35] D. Hwang, E. J. Barron III, A. T. Haque, M. D. Bartlett, *Sci. Rob.* **2022**, *7*, eabg2171.
- [36] H. Liu, H. Tian, X. Li, X. Chen, K. Zhang, H. Shi, C. Wang, J. Shao, *Sci. Adv.* **2022**, *8*, eabn5722.
- [37] H. Okamoto, *J. Phase Equilib. Diffus.* **2004**, *25*, 100.
- [38] F. Li, S. Kuang, X. Li, J. Shu, W. Li, S.-Y. Tang, S. Zhang, *Adv. Mater. Technol.* **2019**, *4*, 1800694.
- [39] G. Yun, S.-Y. Tang, S. Sun, D. Yuan, Q. Zhao, L. Deng, S. Yan, H. Du, M. D. Dickey, W. Li, *Nat. Commun.* **2019**, *10*, 1300.
- [40] H. Wang, Y. Yao, Z. He, W. Rao, L. Hu, S. Chen, J. Lin, J. Gao, P. Zhang, X. Sun, X. Wang, Y. Cui, Q. Wang, S. Dong, G. Chen, J. Liu, *Adv. Mater.* **2019**, *31*, 1901337.
- [41] T. Nishida, Y. Okatani, K. Tadakuma, *Int. J. Humanoid Rob.* **2016**, *13*, 1650017.
- [42] L. Ren, S. Sun, G. Casillas-Garcia, M. Nancarrow, G. Peleckis, M. Turdy, K. Du, X. Xu, W. Li, L. Jiang, S. X. Dou, Y. Du, *Adv. Mater.* **2018**, *30*, 1802595.
- [43] D. C. Kuzma, *Appl. Sci. Res.* **1968**, *18*, 15.
- [44] D. W. Felt, M. Hagenbuchle, J. Liu, J. Richard, *J. Intell. Mater. Syst. Struct.* **1996**, *7*, 589.
- [45] J. C. Martinez-Garcia, A. Serraïma-Ferrer, A. Lopeandía-Fernández, M. Lattuada, J. Sapkota, J. Rodríguez-Viejo, *Nanomaterials* **2021**, *11*, 830.
- [46] J. C. Halpin, *J. Compos. Mater.* **1969**, *3*, 732.
- [47] R. W. Style, R. Boltyanskiy, B. Allen, K. E. Jensen, H. P. Foote, John S. Wettlaufer, E. R. Dufresne, *Nat. Phys.* **2015**, *11*, 82.
- [48] Z. W. Yu, Y. C. Chen, F. F. Yun, X. L. Wang, *Adv. Eng. Mater.* **2017**, *19*, 1700190.
- [49] S. Moon, H. Kim, K. Lee, J. Park, Y. Kim, S. Q. Choi, *iScience* **2021**, *24*, 103183.
- [50] K. Khoshmanesh, S.-Y. Tang, J. Y. Zhu, S. Schaefer, A. Mitchell, K. Kalantar-Zadeh, M. D. Dickey, *Lab Chip* **2017**, *17*, 974.
- [51] A. Lai, P. Thurgood, C. D. Cox, C. Chheang, K. Peter, A. Jaworowski, K. Khoshmanesh, S. Baratchi, *ACS Appl. Mater. Interfaces* **2022**, *14*, 40559.
- [52] Q. Zhao, T. Cole, Y. Zhang, S.-Y. Tang, *Micromachines* **2021**, *12*, 765.
- [53] N. Shi, M. Mohibullah, C. J. Easley, *Annu. Rev. Anal. Chem.* **2021**, *14*, 133.